PNAS RESEARCH ARTICLE | CELL BIOLOGY OPEN ACCESS

Monitoring glycolytic dynamics in single cells using a fluorescent biosensor for fructose 1,6-bisphosphate

John N. Koberstein[a,1], Melissa L. Stewart[a,1], Chadwick B. Smith[a], Andrei I. Tarasov[b], Frances M. Ashcroft[c], Philip J. S. Stork[a], and Richard H. Goodman[a,2]

Contributed by Richard H. Goodman; received March 14, 2022; accepted June 25, 2022; reviewed by John Albeck and Gary Yellen

Cellular metabolism is regulated over space and time to ensure that energy production is efficiently matched with consumption. Fluorescent biosensors are useful tools for studying metabolism as they enable real-time detection of metabolite abundance with single-cell resolution. For monitoring glycolysis, the intermediate fructose 1,6-bisphosphate (FBP) is a particularly informative signal as its concentration is strongly correlated with flux through the whole pathway. Using GFP insertion into the ligand-binding domain of the *Bacillus subtilis* transcriptional regulator CggR, we developed a fluorescent biosensor for FBP termed HYlight. We demonstrate that HYlight can reliably report the real-time dynamics of glycolysis in living cells and tissues, driven by various metabolic or pharmacological perturbations, alone or in combination with other physiologically relevant signals. Using this sensor, we uncovered previously unknown aspects of β-cell glycolytic heterogeneity and dynamics.

glycolysis | β-cells | fructose 1,6-bisphosphate

Significance

Cells respond to shifts in glucose supply or fluctuations in energetic demand through regulated changes in glycolytic metabolism. The rate at which glucose is converted to pyruvate is of considerable importance to cellular physiology; however, measuring this property at single-cell resolution is fundamentally difficult. The glycolytic intermediate fructose 1,6-bisphosphate (FBP) exhibits large changes in concentration that track with changes in flux. We developed a fluorescent biosensor for FBP exploiting this correlation to monitor rapid changes in glycolysis within single cells. HYlight was used in pancreatic β-cells to uncover aspects of glycolytic regulation, dynamics and heterogeneity. Given the conservation and importance of glycolysis, we believe this new biosensor will be broadly useful in a variety of tissues and organisms.

Glycolysis is used by nearly all living organisms for the production of energy and biosynthetic precursors. Given its central role, it is not surprising that the glycolytic pathway, elucidated by Embden, Meyerhof, and Parnas in the 1920s, comprise some of the best-studied reactions in all of biochemistry. Perhaps equally important was the earlier demonstration in 1910 by Harden and Young that orthophosphoric acid, needed for the production of fructose 1,6-bisphosphate (FBP), was required for glycolysis to proceed (1).

FBP production by phosphofructokinase (PFK) sits at an important juncture in the glycolytic pathway and represents the commitment of glucose metabolism to pyruvate formation. Additionally, the final step of glycolysis is catalyzed by pyruvate kinase (PK), one isoform of which is activated by FBP. The kinetics and allosteric regulation of glycolytic enzymes collectively result in a correlation between the concentration of FBP and the overall flux through the pathway (2–4) that has been detected across diverse lifeforms, including bacteria (3), yeast (4), and mammals (5).

The role of FBP in signaling glycolytic flux has perhaps best been demonstrated in the bacterium *Bacillus subtilis*, where the transcription factor CggR (central glycolytic gene repressor) is regulated by FBP binding. In the absence of FBP, CggR represses the expression of multiple glycolytic enzymes (2, 3, 6), thereby allowing FBP to serve as a readout of glycolytic flux induced by glucose availability. Yeast have been engineered that utilize CggR to regulate transcription of a fluorescent protein, thus enabling evaluation of glycolytic flux in single cells by fluorescence microscopy (4). This method is limited, however, by slow kinetics and a lack of subcellular resolution. Similarly, a fluorescence resonance energy transfer (FRET) sensor based on FBP-induced changes in PK quaternization has an extremely narrow dynamic range, limiting its use. Single fluorescent protein biosensors containing a circularly permuted fluorescent protein (cpFP) inserted directly into a ligand-binding domain (LBD), such that ligand binding results in altered fluorescence intensity (7–11), are typically more sensitive than FRET sensors. Here, we describe the development of such a sensor, based on CggR, that can monitor real-time change in intracellular FBP levels in living cells. This biosensor was named HYlight after Harden and Young, the discoverers of FBP.

We chose pancreatic β-cells as a model system because of the essential role of glycolytic metabolism in coupling glucose stimulus to insulin secretion. As in other cells, the elevation of plasma glucose leads to enhanced glycolysis and oxidative phosphorylation. In β-cells, the increase in ATP/ADP ratio subsequently closes ATP-sensitive K^+ (K_{ATP}) channels, triggering plasma membrane electrical activity, Ca^{2+} influx into the cytosol, and insulin secretion (12–14). Notably, β-cell glucose handling is adjusted to sense the substrate availability rather than responding to energy demand, thereby enabling the glucose sensor role for the cell. In particular, glucose uptake is not rate-limiting for glycolytic flux, and glucose phosphorylation is mediated by glucokinase (hexokinase IV), which exhibits a

Author contributions: J.N.K., M.L.S., P.J.S.S., and R.H.G. designed research; J.N.K., M.L.S., C.B.S., and A.I.T. performed research; J.N.K., M.L.S., C.B.S., A.I.T., and F.M.A. analyzed data; A.I.T. and F.M.A. contributed new reagents/analytic tools; and J.N.K., P.J.S.S., and R.H.G. wrote the paper.

Reviewers: J.A., University of California, Davis; and G.Y., Harvard Medical School.

Competing interest statement: P.J.S.S. and J.A. were coauthors on a 2018 conference report.

[1]J.N.K. and M.L.S. contributed equally to this work.

[2]To whom correspondence may be addressed. Email: goodmanr@ohsu.edu.

This article contains supporting information online at http://www.pnas.org/lookup/suppl/doi:10.1073/pnas.2204407119/-/DCSupplemental.

Published July 26, 2022.

higher K_m than other hexokinases and lacks product inhibition (15). These adaptations result in glycolytic flux remaining sensitive to physiologically relevant concentrations of plasma glucose in the millimolar range. Additionally, the low levels of lactate production and transport produce a tight relationship between extracellular glucose and the rates of glycolysis and oxidative metabolism (15). We show here that β-cell FBP levels, monitored by HYlight, increase with glucose concentration in a dose-dependent manner and decrease upon the inhibition of glycolysis, providing compelling evidence that FBP can serve as an indicator of glycolytic flux in these cells. β-Cell lines exhibit metabolic and ionic oscillations, which were detected by HYlight coexpressed with the calcium sensor R-GECO1 (16) in single cells, uncovering the temporal relationship between FBP and Ca^{2+} dynamics.

Finally, we observed an unexpected degree of cell-to-cell heterogeneity in the magnitude of the FBP response upon exposure to glucose present in both MIN6 as well as β-cells within intact islets. Nevertheless, in MIN6 and HEK293 cells, FBP levels averaged across a population of cells recapitulated the well-established importance of glucokinase and hexokinase as regulators of glycolytic rate.

Results

Development of the FBP Biosensor HYlight. To construct our sensor, we used a truncation of *B. subtilis* CggR (residues 89 to 340) (Fig. 1*A* and *SI Appendix*, Fig. S1*A*) that excludes the N-terminal DNA-binding domain (residues 1 to 88) to prevent unnecessary DNA binding (6). We used a cpGFP variant derived from a series of maltose biosensors (9, 10). High-throughput assays were used to characterize the brightness and dynamic range for libraries containing random variations in the site of GFP insertion and composition of the linker amino acids (Fig. 1*B*).

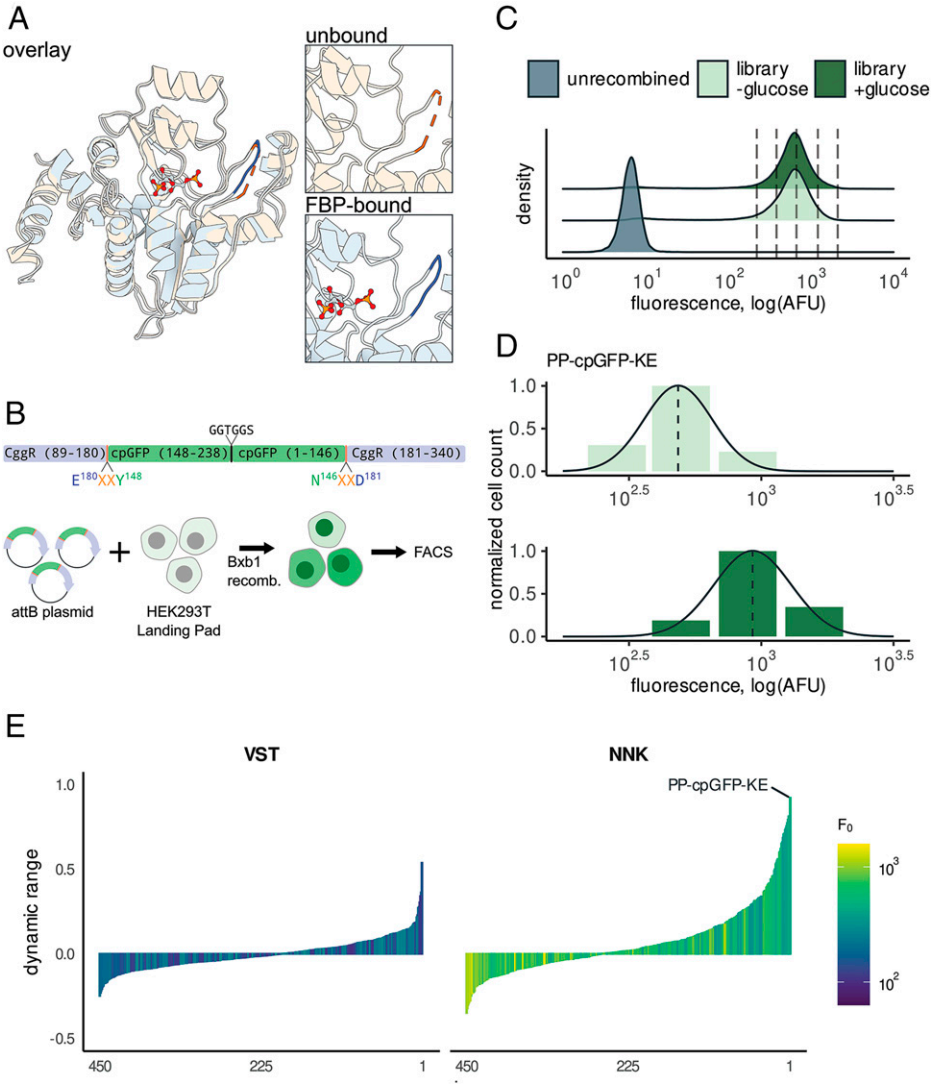

Fig. 1. Discovery of a high dynamic-range FBP biosensor by sort-seq assay. (*A*) Structural comparison of CggR in apo state (PDB ID code 2OKG, orange) vs. FBP bound (PDB ID code 3BXF, blue) reveals a loop (residues 177 to 183) that undergoes a disorder-to-order transition upon binding FBP (6). (*B*) A library of linker variants were assayed for function in HEK293T Landing Pad cells. Circularly permuted GFP was inserted into CggR at residue 180 with two flanking linker amino acids on either side. Linker amino acids were encoded by the degenerate codon VST, which translates to a limited set of 8 amino acids, or by the fully degenerate codon NNK, which includes all 20 amino acids. The library was placed into an attB plasmid that enables genomic recombination into the HEK293T Landing Pad genome by the Bxb1 recombinase. (*C*) Fluorescence distributions of the CggR-180-NNK library expressed in HEK293T cells exposed to 0 mM or 25 mM glucose. Dotted lines indicate the bins used for sort-seq. (*D*) The number of cells sorted into each bin is indicated by bar height along with the maximum-likelihood density estimates for the variant with the highest dynamic range, CggR-180-PP-cpGFP-KE (HYlight). (*E*) Dynamic-range ($\Delta F/F$) estimates for all variants after screening libraries with linker residues substituted with amino acids encoded by a limited set using VST codons (*Left*) or fully degenerate NNK codons (*Right*). See also *SI Appendix*, Fig. S1.

To measure the FBP-induced changes in fluorescence for hundreds of sequence variants in parallel, we utilized sort-seq, a high-throughput functional assay combining fluorescence-activated cell sorting (FACS) and DNA sequencing (17–19). To ensure that expression was limited to a single sequence variant per cell (a requirement of this assay) we employed the HEK293T Landing Pad cell line, which enables genomic integration of the DNA library into a single Bxb1 recombination site (Fig. 1*B*) (20). To characterize FBP-induced changes in fluorescence, we performed sort-seq assays in the presence and absence of 25 mM glucose, which produces high and low intracellular FBP concentrations, respectively. Recombined cells were sorted into four bins spanning the range of the observed library fluorescence intensity (Fig. 1*C* and *SI Appendix*, Fig. S1*B*). Read counts for variants in each bin generated by DNA sequencing provided a view of the log-normal fluorescence distribution analogous to a histogram, from which the mean was inferred using a maximum-likelihood estimator (Fig. 1*D*). Biosensor dynamic range [$\Delta F/F = (F_{ligand} - F_{min})/F_{min}$] was then calculated as the relative difference between the estimated mean fluorescence in the glucose fed (F_{ligand}) and starved (F_{min}) states for each variant.

A key challenge of biosensor design is identifying a site in which cpGFP insertion is tolerated, allowing both domains to fold, while also potentially permitting allosteric coupling between ligand binding and fluorescence. Initially, multiple CggR positions (156 of 251 possible) were tested for permissibility of cpGFP insertion using a transposon-mediated domain-insertion cloning strategy called Domain Insertion Profiling (*SI Appendix*, Fig. S1*A*). None of the insertion-site variants responded to changes in glucose ($|\Delta F/F| < 0.3$ for all tested insertion-site variants) (*SI Appendix*, Fig. S1*C* and Dataset S1). Nonetheless, insertions into the loop comprising residues 177 to 183 (numbered according to the full-length protein) were relatively bright compared to the other tested sites ($F_{min} = 2.1 \pm 0.04$ logAFU, $P < 0.005$ Mann–Whitney U test), prompting us to focus on this region. Structures of the CggR LBD in the apo- and FBP-bound states indicated that this loop undergoes an FBP-dependent disordered-to-ordered transition (Fig. 1*A*). To minimize disruption of the FBP-binding site, we placed cpGFP at the apex of the loop for further optimization of linker amino acids.

Only a fraction of the possible linkers will produce strong allosteric coupling between a given cpFP and LBD. We designed a library containing cpGFP inserted between residues 180 and 181 of CggR with short linkers on either side consisting of two amino acids each (Fig. 1*B*). The linker amino acids were encoded by either the degenerate codons VST (amino acids A, G, P, R, S, T) or NNK (all 20 amino acids). The NNK library contains a greater number of combinations ($20^4 = 160{,}000$) than what could readily be characterized. To reduce the number of combinations to an experimentally tractable number, 10,000 cells from the top 10% by brightness were sorted in the presence of glucose, expanded, and used as input for subsequent assays using this library.

After filtering out low-abundance variants and those outside the expected range, we estimated the brightness and dynamic range for 900 linker variants between the two linker libraries (Fig. 1*E* and Dataset S1). Although most variants did not display glucose-dependent alterations in fluorescence, both libraries contained rare variants that showed large fluorescence changes. The fully degenerate NNK library produced more high dynamic-range variants than the more limited VST library (Fig. 1*E*). Notably, biosensors with fluorescence increases (turn-on) and decreases (turn-off) upon addition of glucose were both identified (Fig. 1*E*). The variant with the largest dynamic range ($\Delta F/F = 0.92$) contained the linker pairs Pro-Pro and Lys-Glu on the N- and C-terminal ends of cpGFP, respectively. This variant, named HYlight, was used to explore FBP dynamics in vitro and in live pancreatic β-cells.

In Vitro Characterization of HYlight. When excited by 488-nm light, purified HYlight protein exhibited an increase in emission at 510 nm with increasing [FBP] ($\Delta F/F = 1.5$) (Fig. 2 *A*–*C*). An additional major excitation peak was discovered at 400 nm, which produced a slightly red-shifted emission (Fig. 2*B*). This latter signal decreased with increasing [FBP] (Fig. 2 *A*–*C*). The ratio of the emission values from the two excitation wavelengths provided a readout with increased sensitivity ($\Delta R/R = 3.0$) (Fig. 2*D*) and reduced variability resulting from differences in biosensor concentration (*SI Appendix*, Fig. S2*A*) and pH (Fig. 2*E* and *SI Appendix*, Fig. S2*B*). Excitation at 400 nm is a characteristic of wtGFP caused by excited state proton transfer (ESPT) from the neutral state of the fluorophore to nearby residues (21). Given that the cpGFP used in HYlight contains the well-characterized mutation S65T that disrupts EPST when introduced into wtGFP, we hypothesized that a relatively uncommon mutation present in HYlight, H148Y, might contribute to the strong excitation at 400 nm due to the proximity of this residue to fluorophore. Reverting this mutation back to the wild-type His148 indeed produced a biosensor with significantly diminished 400-nm excitation (*SI Appendix*, Fig. S2*C*).

The apparent affinity of HYlight for FBP (11 μM) (*SI Appendix*, Fig. 2*D*) (variability among batches of purified protein resulted in K_d estimates ranging from 3.8 to 12.5 μM) is comparable to previously reported measurements by isothermal calorimetry using only the CggR LBD (6). However, this binding is tighter than that reported using the full-length protein in thermal-shift assays (2, 4). The range of FBP concentrations sensed by HYlight in vitro (~1 μM to 100 μM) is well suited for the range of FBP concentrations measured in a β-cell line stimulated by 11 mM glucose following starvation (22). However, metabolomic measurements in mammalian iBMK cells continuously cultured in high glucose indicate that FBP is present at 1.5 mM (23). Given this discrepancy, it is possible that HYlight binding could be saturated in some contexts or cell types.

While binding to FBP has been well characterized, it has not been determined whether CggR also binds fructose 2,6-bisphosphate (F2,6BP), which is not produced in *B. subtilis* but is present in eukaryotic cells at much lower concentrations than FBP. F2,6BP affected HYlight fluorescence similarly to FBP but with slightly weaker affinity (*SI Appendix*, Fig. S2*D*) (K_d = 7.2 μM for F2,6BP and 3.8 μM for FBP). Given the considerably lower cytosolic concentration of F2,6BP, it is unlikely that it influences the observed fluorescence in cells.

To examine HYlight specificity, we tested other glycolytic metabolites, namely dihydroxyacetone phosphate (DHAP), glyceraldehyde 3-phosphate (G3P), fructose 6-phosphate (F6P), glucose 6-phosphate (G6P), and glucose. Minimal changes in the HYlight fluorescence ratio were observed in the presence of supraphysiological concentrations of these other metabolites (Fig. 2*F*). The absence of a fluorescence response to other ligands does not necessarily preclude binding, however. In the presence of 100 μM F6P, 675 μM G6P, or 1.6 mM DHAP, the FBP dose–response curve for HYlight was shifted rightward, suggesting competition for the same binding site (*SI Appendix*, Fig. S2*E*). When combined, these competing ligands produce a larger shift in the K_d of HYlight for FBP to 33.0 μM (*SI Appendix*, Fig. S2*E*). Competition for the binding site precludes HYlight from reporting absolute concentrations and may enable HYlight to

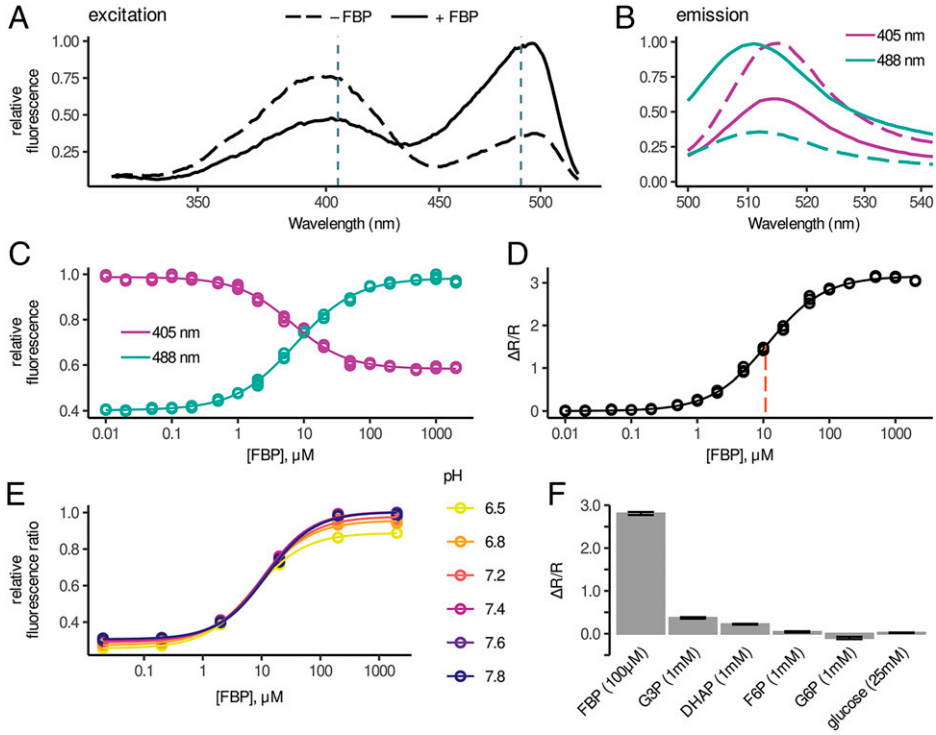

Fig. 2. In vitro characterization of HYlight. (*A*) Excitation spectra from HYlight in the presence (solid) and absence (dashed) of 1 mM FBP. (*B*) Emission spectra from HYlight in the presence and absence of 1 mM FBP. Dashed lines indicate excitation set at 405 nm while solid lines indicate excitation set at 488 nm. (*C*) Normalized HYlight emission induced by excitation at 405 nm (purple) or 488 nm (cyan) as a function of FBP concentration. (*D*) Relative change of the fluorescence ratio ($\Delta R/R$) resulting from 488- and 405-nm excitation as a function of [FBP]. (*E*) Fluorescence ratio as a function of pH across FBP concentrations. (*F*) Relative HYlight fluorescence ratio for FBP compared to other glycolytic metabolites. See also *SI Appendix*, Fig. S2.

sense higher FBP levels than those suggested from the K_d determined in vitro.

While the fluorescence ratio of HYlight is largely insensitive to pH, this results from similar changes in fluorescence intensity for both 405- and 488-nm excitation across the pH range tested. As an additional control, we generated a variant incapable of binding FBP. We hypothesized that replacing the CggR residue Thr152 with Glu would result in the charged side chain of Glu occupying the region of the binding site normally occupied by the 6-phosphate. This T152E variant exhibited no changes in fluorescence ratio across FBP concentrations (*SI Appendix*, Fig. S2*B*). In addition, the T152E variant exhibited similar sensitivity to pH changes as HYlight. This "binding dead" HYlight was used as an experimental control to detect artifactual changes in fluorescence caused by factors other than FBP.

In Vivo Characterization of HYlight. We examined the relationship between the extracellular glucose and intracellular FBP levels by measuring HYlight fluorescence in live HEK293 cells and insulin-secreting MIN6 β-cells using flow cytometry. Fluorescence was monitored using 405- and 488-nm excitation and the relative change ($\Delta R/R_0$) in fluorescence ratio ($R = F_{488}/F_{405}$) was calculated relative to the no glucose condition (R_0). In both cell types, the median $\Delta R/R_0$ exhibited a glucose-dependent increase, but the concentration of glucose that elicited a half-maximal $\Delta R/R_0$ ($R_{0.5}$) differed between cell types (Fig. 3 *A* and *B*). In MIN6 cells, $R_{0.5}$ was achieved at 6.4 ± 1.6 mM glucose (Fig. 3*B*), which is close to the glucose concentration reported for half-maximal activation of glucokinase (24). In contrast, the $R_{0.5}$ occurred at a much lower glucose concentration in HEK293 cells (1.0 ± 0.2 mM glucose, $P < 0.05$ vs. MIN6). This is consistent with a key role for hexokinase (HKI $K_{0.5}$ = 41 μM, HKII $K_{0.5}$ = 340 mM) and a lack of glucokinase in HEK293 cells (25, 26). The glucokinase activator dorzagliatin (10 μM) significantly lowered the concentration eliciting half-maximal activation ($R_{0.5}$ = 1.7 ± 0.4 mM glucose, $P < 0.05$ vs. untreated cells) in MIN6 cells.

HYlight Can Differentiate Cell Types Based on Response to Metabolic Perturbations. We next examined the use of HYlight for detecting cell type-specific differences in FBP dynamics in HEK293 and MIN6 cells monitored by time-lapse confocal microscopy (Fig. 3*C*). Cells were starved of glucose for 1 h prior to imaging, followed by the sequential addition of 11 mM glucose, 2.5 μM oligomycin, and 16.7 mM 2-deoxyglucose (2-DG) to mimic a common Seahorse XF protocol referred to as the Glycolytic Stress Test. Fluorescence was monitored using 405- and 488-nm excitation and the change in fluorescence ratio ($\Delta R/R_0$) was calculated relative to the ratio at the start of experiment (R_0). In response to 11 mM glucose, HEK293 cells exhibited a transient spike in fluorescence ratio, which rapidly declined to a steady plateau ($\Delta R/R$ = 0.41 ± 0.20) (Fig. 3 *C* and *D*), possibly due to ATP feedback inhibition of PFK. The glucose-induced increase in fluorescence ratio exhibited a slower increase but plateaued at a higher level in MIN6 cells ($\Delta R/R$ = 0.83 ± 0.19, $P < 0.05$ vs. HEK293 cells) (Fig. 3*D*). In contrast, glucose-starved MIN6 cells expressing the HYlight-T152E variant exhibited no change in fluorescence ratio upon exposure to 11 mM glucose (*SI Appendix*, Fig. S3). Oligomycin, an inhibitor of the mitochondrial ATP-synthase, produced a further, sustained increase in fluorescence ratio in HEK293 cells, presumably reflecting an increased anaerobic glycolytic capacity of HEK293 cells when oxidative phosphorylation is inhibited. In contrast, the glucose-induced increase in fluorescence ratio was largely reversed by oligomycin in MIN6 cells. This likely reflects the inability of β-cells to metabolize glucose to lactate (27, 28), which results in insufficient glycolytic ATP for FBP production by PFK. Finally,

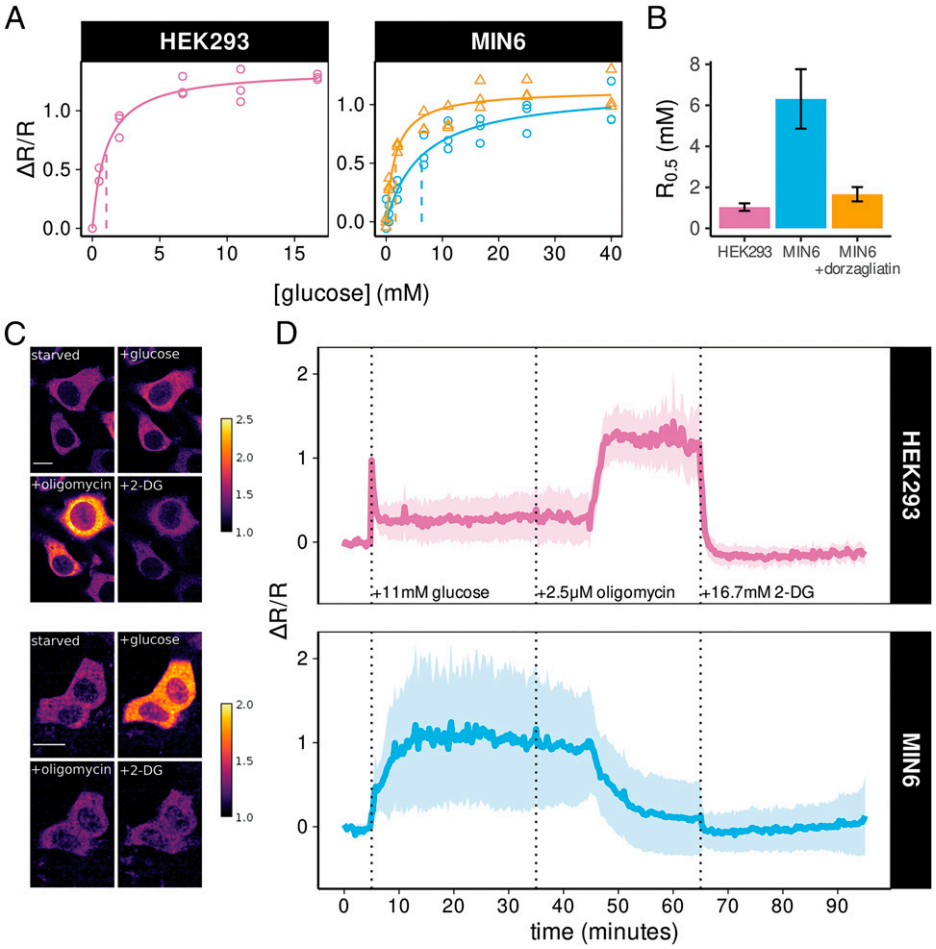

Fig. 3. HYlight imaging reveals differences in metabolic phenotype between HEK293 and MIN6 cells. (*A*) HYlight fluorescence ratio as a function of glucose concentration follows Michaelis–Menten kinetics. Differences in the magnitude of maximal change and $R_{0.5}$ are observed between HEK293 (purple), MIN6 (blue), and MIN6 cells treated with dorzagliatin (orange). Each point represents the median fluorescence ratio across cells measured by flow cytometry relative to cells incubated in 0 mM glucose. Lines indicate fitted Michaelis–Menten equation with $R_{0.5}$ shown as a vertical dashed line. (*B*) Comparison of $R_{0.5}$ estimates ± SE for HEK293 (1.0 ± 0.24 mM), MIN6 (6.4 ± 1.6mM), and MIN6 cells treated with 10 μM dorzagliatin (1.28 ± 0.22 mM). (*C*) Example of fluorescence ratiometric images in HEK293 cells (*Upper*) and MIN6 cells (*Lower*) after 1 h of glucose starvation and following addition of 11 mM glucose, 2.5 μM oligomycin, and 16.7 mM 2-DG. The scale bars in the photomicrographs represent 10 microns. (*D*) Quantification of the change in fluorescence ratio (Δ*R*/*R*) for HEK293 cells (*Upper*, $n = 67$ cells over 3 separate experiments) and MIN6 cells (*Lower*, $n = 222$ cells over 3 separate experiments) following the metabolic perturbations shown in *C*. Δ*R*/*R* was normalized to the glucose-starved state at the beginning of each experiment. Solid line represents the mean across cells while shaded ribbon represents the mean ± SD. In MIN6 cells, oscillations around the mean contribute to the increased cell-to-cell variability in fluorescence ratio over time. See also *SI Appendix*, Fig. S3.

2-DG reduced glycolysis in HEK293 cells, as evidenced by a rapid decline in fluorescence ratio back to baseline (Fig. 3*D*), while only minimally decreasing the already low FBP levels in MIN6 cells.

Multiplexed Imaging with HYlight Resolves Temporal Relationship between Oscillating Signals. In addition to the sustained increase in FBP upon exposure of MIN6 cells to 11 mM glucose, HYlight also uncovered large amplitude oscillations in FBP, consistent with properties of a glycolytic oscillator (29). β-Cell lines are known to exhibit glucose-induced oscillations in plasma membrane electrical potential and cytosolic Ca^{2+}, but the temporal relationship between ionic and glycolytic oscillations is unclear. We examined the relationship between FBP and Ca^{2+} dynamics in individual MIN6 cells by coexpressing HYlight and a spectrally compatible Ca^{2+} sensor, R-GECO1 (16). As expected, the initial increase in FBP stimulated by glucose preceded the increase in Ca^{2+} (Fig. 4 *A* and *B*). The glucose-induced oscillations of FBP and Ca^{2+} in individual cells were in phase, with a periodicity of ∼60 s (Fig. 4*C*). Cross-correlation analysis of the two signals averaged over all cells indicated the two signals were maximally correlated with little (15 s) or no time offset (Fig. 4*D*).

HYlight Reveals Differences in Glycolytic Dynamics at the Single-Cell Level in Intact Islets. A key advantage of fluorescent biosensor imaging is the high spatial resolution, which permits evaluation of the metabolic properties of single cells. In MIN6 β-cells, the FBP response to elevated glucose was highly heterogeneous (Figs. 3*D* and 4*A*). Glucose-induced increases in FBP were also readily detected in individual β-cells within isolated mouse islets expressing HYlight, delivered via a β-cell specific adeno-associated virus (AAV) vector. As in MIN6 cells, the individual FBP responses of primary islet β-cells were heterogeneous (Fig. 5 *A* and *B*). To determine whether the variability in FBP response in individual cells persisted over multiple stimulations, we treated islets with cycles of low (1 mM) and high (11 mM) glucose. The per cell magnitude of HYlight increase was highly correlated between sequential rounds of glucose stimulation ($R = 0.75$) (Fig. 5*C*).

Discussion

We developed HYlight to monitor FBP dynamics with cellular resolution, an effort motivated by a growing appreciation for the role of this metabolite in reflecting the state of the

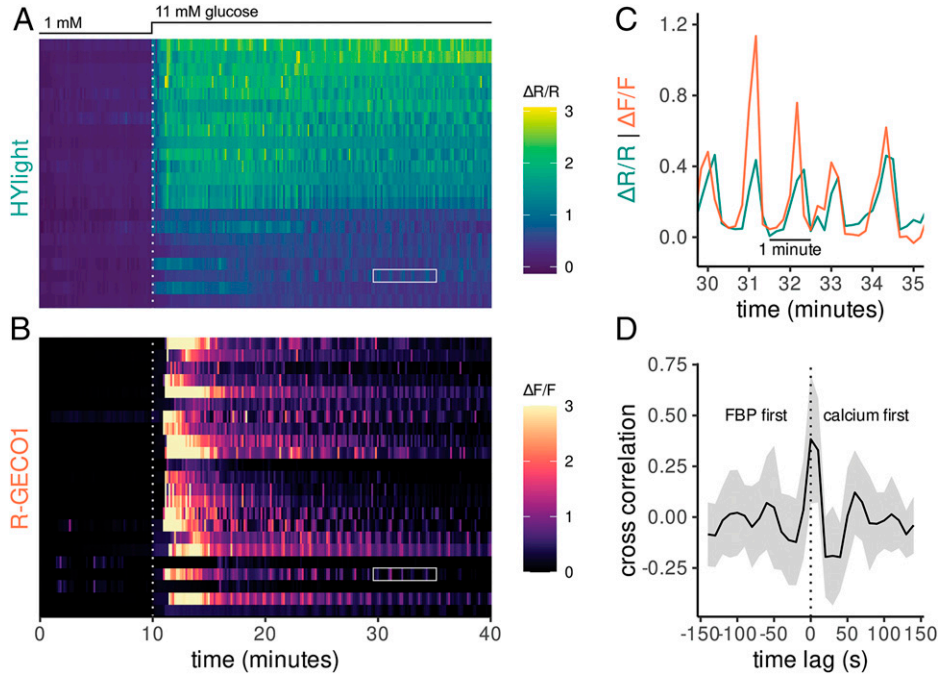

Fig. 4. Multiplexed fluorescence imaging of HYlight and R-GECO uncovers temporal relationships between FBP and Ca^{2+} in MIN6 cells. (*A*) HYlight fluorescence ratio measured in MIN6 cells following an increase from 1 to 11 mM glucose. (*B*) R-GECO fluorescence measured in the same cells as *A* revealed a delayed increase in Ca^{2+} relative to FBP. (*C*) The HYlight fluorescence ratio and R-GECO fluorescence for a single cell indicated by white boxes in *A* and *B*. Oscillations in both signals occur synchronously. (*D*) The cross-correlation of R-GECO and HYlight signal following glucose stimulation (t = 20 to 40 min) averaged over all cells with a shaded ribbon representing the mean ± the SD. The maximum cross-correlation occurs in simultaneous frames or at a one-frame (15 s) lag with the R-GECO signal preceding HYlight.

glycolytic pathway. CggR, a transcription factor that enables bacteria to sense and respond to changes in glycolytic flux, was utilized to engineer our sensor via high-throughput functional assays in live cells. Inserting cpGFP into a loop of CggR that undergoes a structural transition with ligand binding produced a relatively bright construct, but one that lacked responsiveness to FBP. High-throughput characterization of the linker amino acids connecting cpGFP to CggR revealed multiple high dynamic-range FBP biosensors. Given that only 900 of the 160,000 possible linker amino acid combinations were tested, it is likely that linker variants with improved performance remain undiscovered. The many pairs of biosensor sequence and associated dynamic range collected in this study might prove useful as training data for emerging machine-learning methods to predict the function for untested sequences. Moreover, the ratiometric signal and high dynamic range of HYlight combined with the large changes in FBP that track with alterations of flux (30) make this sensor an especially useful tool for

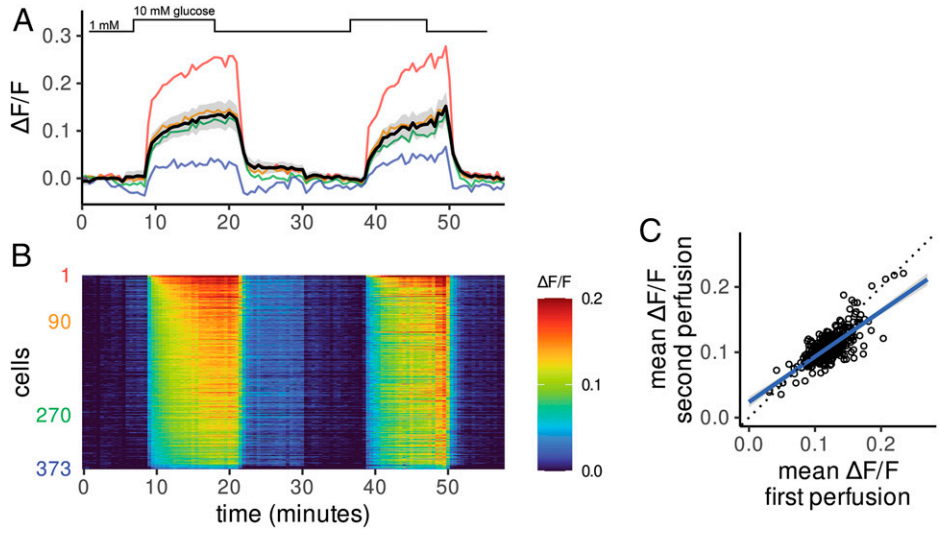

Fig. 5. HYlight uncovers heterogeneity among β-cells in response to glucose. (*A*) β-Cells within an isolated islet imaged with repeated cycling between 1 and 10 mM glucose. The solid black line and the gray-shaded region represent the mean ± SD, respectively. Four traces from example cells are shown as colored lines corresponding to the maximum (red) and minimum (blue) glucose-stimulated fluorescence change along with two cells exhibiting intermediates responses (orange and green). (*B*) Heatmap of fluorescence changes (Δ*F*/*F* represented by color) where each row represents a single cell quantified over time. Cells are ordered from numerical ranks on the *y* axis. (*C*) The mean change in fluorescence ratio during the first and second exposure to 10 mM glucose is heterogeneous across cells but consistent within individual cells over time (R = 0.75). The blue line represents a linear regression fit, while dotted black indicates the unity line.

monitoring metabolism in live cells. HYlight thus complements existing fluorescent biosensors covering the major glycolytic pathway inputs [glucose (31)], outputs [pyruvate (32) and lactate (33, 34)], and cofactors [NAD^+:NADH (35) and ATP:ADP (8)].

Pancreatic β-cells, whose glycolytic rate depends on glucose supply, provided an ideal system to test HYlight and an opportunity to detect FBP dynamics in relation to normal physiology. HYlight detected changes in FBP across a range of glucose concentrations in MIN6 cells and isolated islets. Additionally, perturbations thought to increase glycolytic flux, either by increasing glucokinase activity in MIN6 cells or inhibiting mitochondrial function in HEK293 cells, were associated with an increased HYlight fluorescence ratio, providing further evidence that FBP levels reflect glycolytic flux. Different β-cells within the same islet exhibited heterogeneous responses to glucose that were maintained over time, indicating a cell intrinsic source of variability. Despite the high variability in FBP levels among individual HEK293 and MIN6 cells, the median HYlight fluorescence ratio in response to different concentrations of glucose, revealed by flow cytometry, conformed to the known properties of hexokinase and glucokinase. The detection of fast (∼1-min period) oscillations in FBP in MIN6 cells, in synchrony with those of Ca^{2+} likely reflects the hierarchy of metabolic and electrical signaling in the β-cell. The concurrence of FBP and Ca^{2+} peaks that we observed contrasts with prior studies using PKAR, a considerably less-sensitive FRET sensor for PKM2 tetramerization, which showed, also in MIN6 cells, that FBP oscillated out of phase with Ca^{2+} (36).

Beyond the example of β-cells, HYlight should be useful for monitoring glycolysis across a range of cell types, tissues, and organisms. Precise measurement of glycolytic flux, however, requires metabolic labeling followed by destructive analytical chemistry techniques (37). To monitor metabolic flux in live cells, instruments that measure the rate of oxygen consumption and extracellular acidification have been developed, most notably the Seahorse XF analyzer (37). However, these methods are limited to measuring bulk properties of cell populations, thereby obscuring the heterogeneity among individual cells. Additionally, Seahorse assays do not lend themselves to perfusion experiments, making it difficult to assess effects of removing an agent. While HYlight measurement of FBP does not provide absolute quantification of flux, our qualitative findings from flow cytometry and fluorescence microscopy reflect the known metabolic properties elucidated through bulk assays, with enhanced spatiotemporal resolution. These advantages, combined with the relative affordability and flexibility of a fluorescent biosensor, suggest that HYlight could be broadly useful for metabolic assays in a wide variety of biological contexts.

In cancer biology, it has become apparent that cellular metabolic heterogeneity contributes to disease progression and therapeutic response. The preference of cancer cells for aerobic fermentation (Warburg effect) varies from cell to cell in solid tumors, depending on the level of hypoxia and interactions with the tumor microenvironment (38, 39). Imaging of HYlight-expressing cells using a fluorescence microscope should be able to detect metabolic characteristics of individual cells. Additionally, subcellular compartmentalization of glycolysis, well-known in trypanosomes, where glycolytic enzymes are segregated into discrete organelles, and yeast, where glycolytic enzymes are enriched in liquid condensates known as G bodies, is emerging as an important response of neurons to activity-dependent energy demands (40, 41). We anticipate that HYlight will be useful in characterizing glycolytic regulation at the subcellular level in addition to the examples provided in the present work.

Materials and Methods

Detailed descriptions of all materials and methods are available in *SI Appendix*. All primer sequences can be found in *SI Appendix*, Table S1. Information related to fluorescence activated cell sorting experiments can be found in *SI Appendix*, Table S2.

FACS. Sort-seq experiments were conducted using a BD Influx instrument. Cells transfected with the biosensor library (CggR-DIP or CggR-180-VST/NNK) and Bxb1 recombinase were sorted to collect GFP^+, BFP^- cells. For second-round FACS, four equal-width gates were set to span the range of log(AFU) covered by the distribution of each library. The ± glucose samples were sorted using the same gates for ∼1.5 h each. Cells for each bin were collected, individually pelleted, resuspended, and plated for expansion. Genomic DNA from 5 M cells was extracted.

Linker Library DNA Sequencing. The entire ORF was PCR-amplified with a forward primer specific to the genome and a reverse primer in sequence derived from the plasmid. The linker regions flanking cpGFP were PCR amplified in a second round to add partial Illumina adapters and then amplified a third time with primer i5-IPE2p and a unique indexed primer per sample (i7- iPE2p-XX). The library was sequenced using 2 × 75-bp paired-end reads on an Illumina MiSeq (v3 Reagent kit) loaded at a final concentration of 14 pM with 15% PhiX spiked in.

Imaging and Quantification. One hour prior to imaging, HEK293 or MIN6 cells were glucose starved (0 mM or low glucose, 145 mM NaCl, 5 mM KCl, 1.2 mM $MgCl_2$, 2.6 mM $CaCl_2$, 10 mM Hepes, pH 7.4). Live cells were imaged on a Nikon Eclipse TiE inverted microscope with a Yokogawa CSU-W1 spinning disk confocal unit and a 60× oil-based objective (NA 1.4, Plan Apo VC OFN 25) using the perfect focus system. Cells were excited at 488 nm and 405 nm with emission wheel 525/25 nm and maintained in 5% CO_2 at 37 °C. Intracellular FBP in islets was reported by exciting HYlight at 485 nm with emission at 515nm using a Zeiss Axiozoom.V16 microscope (2.3/0.56 objective) or Zeiss Axioskop microscope (20/1.0 objective).

Flow Cytometry. MIN6 cells were transduced with a β-cell–specific AAV encoding HYlight. HEK293T were transfected using Lipofectamine 2000. All cells were incubated with 5% CO_2 at 37 °C for 24 to 48 h. One hour prior to harvest, MIN6 or HEK293 culture media was exchanged for media containing 145 mM NaCl, 5 mM KCl, 1.2 mM $MgCl_2$, 2.6 mM $CaCl_2$, 10 mM Hepes, and glucose ranging from 0 to 25 mM. Dorzagliatin (10 μM, Selleckchem, Cat. #S6921) was added for 1 h. Cells were trypsinized, pelleted, and resuspended in media containing the same concentration of glucose prior to harvest, with or without dorzagliatin. Cells were kept at room temperature. Data were collected on a BD Symphony Flow Cytometer using lasers 488-1 (excitation 488 nm, Emission 530/30 nm) and 405-2 (excitation 405 nm, emission 525/50 nm).

Data Availability. All study data are included in the main text and supporting information.

ACKNOWLEDGMENTS. We thank Markus Grompe and Sunghee Chai for the β-cell–specific adeno-associated virus vector; Xander Viray and James Frank for help with calcium measurements; Matthew Schleisman for assistance with FACS; Yibing Jia for help with DNA sequencing; Stephanie Kaech for her expertise in microscopy; Erkan Karakas and Carsten Shultz for helpful discussions; and Paul Klevit and Melissa Kirigiti from the Oregon National Primate Research Center for technical assistance in preparing islets. Portions of this work were carried out in the Oregon Health and Science University Imaging Core, Flow Cytometry Core, Molecular Technologies Core, and by R01 AG055431 (to R.H.G.).

Author affiliations: [a]Vollum Institute, Oregon Health & Science University, Portland, OR 97239; [b]School of Biomedical Sciences, Ulster University, Coleraine BT52 1SA, United Kingdom; and [c]Department of Physiology, Anatomy, and Genetics, University of Oxford, Oxford OX1 3PT, United Kingdom

1. A. Harden, W. Young, The alcoholic ferment of yeast-juice. *Proc. Royal Soc. B* **77**, 405–420 (1906).
2. B. Bley Folly *et al.*, Assessment of the interaction between the flux-signaling metabolite fructose-1,6-bisphosphate and the bacterial transcription factors CggR and Cra. *Mol. Microbiol.* **109**, 278–290 (2018).
3. K. Kochanowski *et al.*, Functioning of a metabolic flux sensor in Escherichia coli. *Proc. Natl. Acad. Sci. U.S.A.* **110**, 1130–1135 (2013).
4. F. Monteiro *et al.*, Measuring glycolytic flux in single yeast cells with an orthogonal synthetic biosensor. *Mol. Syst. Biol.* **15**, e9071 (2019).
5. L. B. Tanner *et al.*, Four key steps control glycolytic flux in mammalian cells. *Cell Syst.* **7**, 49–62.e8 (2018).
6. P. Rezácová *et al.*, Crystal structures of the effector-binding domain of repressor central glycolytic gene regulator from Bacillus subtilis reveal ligand-induced structural changes upon binding of several glycolytic intermediates. *Mol. Microbiol.* **69**, 895–910 (2008).
7. G. S. Baird, D. A. Zacharias, R. Y. Tsien, Circular permutation and receptor insertion within green fluorescent proteins. *Proc. Natl. Acad. Sci. U.S.A.* **96**, 11241–11246 (1999).
8. J. Berg, Y. P. Hung, G. Yellen, A genetically encoded fluorescent reporter of ATP:ADP ratio. *Nat. Methods* **6**, 161–166 (2009).
9. J. S. Marvin, E. R. Schreiter, I. M. Echevarría, L. L. Looger, A genetically encoded, high-signal-to-noise maltose sensor. *Proteins* **79**, 3025–3036 (2011).
10. D. C. Nadler, S. A. Morgan, A. Flamholz, K. E. Kortright, D. F. Savage, Rapid construction of metabolite biosensors using domain-insertion profiling. *Nat. Commun.* **7**, 12266 (2016).
11. J. Nakai, M. Ohkura, K. Imoto, A high signal-to-noise Ca(2+) probe composed of a single green fluorescent protein. *Nat. Biotechnol.* **19**, 137–141 (2001).
12. F. M. Ashcroft, D. E. Harrison, S. J. Ashcroft, Glucose induces closure of single potassium channels in isolated rat pancreatic beta-cells. *Nature* **312**, 446–448 (1984).
13. D. G. Nicholls, The pancreatic β-cell: A bioenergetic perspective. *Physiol. Rev.* **96**, 1385–1447 (2016).
14. P. Rorsman, F. M. Ashcroft, Pancreatic β-cell electrical activity and insulin secretion: Of mice and men. *Physiol. Rev.* **98**, 117–214 (2018).
15. F. M. Matschinsky, D. F. Wilson, The central role of glucokinase in glucose homeostasis: A perspective 50 years after demonstrating the presence of the enzyme in islets of Langerhans. *Front. Physiol.* **10**, 148 (2019).
16. Y. Zhao *et al.*, An expanded palette of genetically encoded Ca^{2+} indicators. *Science* **333**, 1888–1891 (2011).
17. J. B. Kinney, A. Murugan, C. G. Callan Jr., E. C. Cox, Using deep sequencing to characterize the biophysical mechanism of a transcriptional regulatory sequence. *Proc. Natl. Acad. Sci. U.S.A.* **107**, 9158–9163 (2010).
18. J. N. Koberstein, M. L. Stewart, T. L. Mighell, C. B. Smith, M. S. Cohen, A sort-seq approach to the development of single fluorescent protein biosensors. *ACS Chem. Biol.* **16**, 1709–1720 (2021).
19. N. Peterman, E. Levine, Sort-seq under the hood: Implications of design choices on large-scale characterization of sequence-function relations. *BMC Genomics* **17**, 206 (2016).
20. K. A. Matreyek, J. J. Stephany, M. A. Chiasson, N. Hasle, D. M. Fowler, An improved platform for functional assessment of large protein libraries in mammalian cells. *Nucleic Acids Res.* **48**, e1 (2020).
21. H. Lossau *et al.*, Time-resolved spectroscopy of wild-type and mutant green fluorescent proteins reveals excited state deprotonation consistent with fluorophore-protein interactions. *Chem. Phys.* **213**, 1–16 (1996).
22. H. K. Berman, C. B. Newgard, Fundamental metabolic differences between hepatocytes and islet beta-cells revealed by glucokinase overexpression. *Biochemistry* **37**, 4543–4552 (1998).
23. J. O. Park *et al.*, Metabolite concentrations, fluxes and free energies imply efficient enzyme usage. *Nat. Chem. Biol.* **12**, 482–489 (2016).
24. F. M. Matschinsky, Regulation of pancreatic beta-cell glucokinase: From basics to therapeutics. *Diabetes* **51** (suppl. 3), S394–S404 (2002).
25. A. E. Aleshin *et al.*, Crystal structures of mutant monomeric hexokinase I reveal multiple ADP binding sites and conformational changes relevant to allosteric regulation. *J. Mol. Biol.* **296**, 1001–1015 (2000).
26. H. Ardehali *et al.*, Functional organization of mammalian hexokinase II. Retention of catalytic and regulatory functions in both the NH2- and COOH-terminal halves. *J. Biol. Chem.* **271**, 1849–1852 (1996).
27. N. Sekine *et al.*, Low lactate dehydrogenase and high mitochondrial glycerol phosphate dehydrogenase in pancreatic beta-cells. Potential role in nutrient sensing. *J. Biol. Chem.* **269**, 4895–4902 (1994).
28. C. Zhao, M. C. Wilson, F. Schuit, A. P. Halestrap, G. A. Rutter, Expression and distribution of lactate/monocarboxylate transporter isoforms in pancreatic islets and the exocrine pancreas. *Diabetes* **50**, 361–366 (2001).
29. V. N. Civelek, J. T. Deeney, G. E. Fusonie, B. E. Corkey, K. Tornheim, Oscillations in oxygen consumption by permeabilized clonal pancreatic beta-cells (HIT) incubated in an oscillatory glycolyzing muscle extract: Roles of free Ca2+, substrates, and the ATP/ADP ratio. *Diabetes* **46**, 51–56 (1997).
30. M. A. Lorenz, M. A. El Azzouny, R. T. Kennedy, C. F. Burant, Metabolome response to glucose in the β-cell line INS-1 832/13. *J. Biol. Chem.* **288**, 10923–10935 (2013).
31. J. P. Keller *et al.*, In vivo glucose imaging in multiple model organisms with an engineered single-wavelength sensor. *Cell Rep.* **35**, 109284 (2021).
32. R. Arce-Molina *et al.*, A highly responsive pyruvate sensor reveals pathway-regulatory role of the mitochondrial pyruvate carrier MPC. *eLife* **9**, e53917 (2020).
33. A. Galaz *et al.*, Highly responsive single-fluorophore indicator to explore lactate dynamics in high calcium environments. *bioRxiv* [Preprint] (2020). https://www.biorxiv.org/content/10.1101/2020.10.01.322404v1. This version was posted October 2, 2020.
34. Y. Nasu, Y. Shen, L. Kramer, R. E. Campbell, Structure- and mechanism-guided design of single fluorescent protein-based biosensors. *Nat. Chem. Biol.* **17**, 509–518 (2021).
35. Y. P. Hung, J. G. Albeck, M. Tantama, G. Yellen, Imaging cytosolic NADH-NAD(+) redox state with a genetically encoded fluorescent biosensor. *Cell Metab.* **14**, 545–554 (2011).
36. M. J. Merrins, A. R. Van Dyke, A. K. Mapp, M. A. Rizzo, L. S. Satin, Direct measurements of oscillatory glycolysis in pancreatic islet β-cells using novel fluorescence resonance energy transfer (FRET) biosensors for pyruvate kinase M2 activity. *J. Biol. Chem.* **288**, 33312–33322 (2013).
37. T. TeSlaa, M. A. Teitell, Techniques to monitor glycolysis. *Methods Enzymol.* **542**, 91–114 (2014).
38. H. Kondo *et al.*, Single-cell resolved imaging reveals intra-tumor heterogeneity in glycolysis, transitions between metabolic states, and their regulatory mechanisms. *Cell Rep.* **34**, 108750 (2021).
39. D. A. Lawson, K. Kessenbrock, R. T. Davis, N. Pervolarakis, Z. Werb, Tumour heterogeneity and metastasis at single-cell resolution. *Nat. Cell Biol.* **20**, 1349–1360 (2018).
40. S. Jang *et al.*, Glycolytic enzymes localize to synapses under energy stress to support synaptic function. *Neuron* **90**, 278–291 (2016).
41. V. Rangaraju, N. Calloway, T. A. Ryan, Activity-driven local ATP synthesis is required for synaptic function. *Cell* **156**, 825–835 (2014).